Optimization of Single Pitch Error and MRR in a WEDM Gear Cutting Process

Kasinath Das Mohapatra and Susanta Kumar Sahoo

Abstract Gears are the key elements to the manufacturing processes. Gears having teeth or wheels mesh together with other gears to transmit torque. Accurate motion transfer and minimum running noise are the two most important features for these gears which depend on the amount of errors, i.e. the errors present in the pitch of the gears. Gears can be manufactured by different manufacturing processes such as shaping, forming, hobbing, milling and broaching. Gears are one of the crucial components of the highly accurate miniaturized devices such as pumps and motors, electronics, business machines, home appliances, automotive parts, measuring instruments, timing devices, MEMS, etc. It is also used in the scientific, industrial and domestics areas. Gear cutting by WEDM finds its application in many industrial areas of aeronautical and electrical industries that requires precise finishing and appropriate accuracy. Geared devices can change the torque, speed and direction of the power source. Copper, bronze, brass, stainless steel and aluminium are the most frequently used materials for these gears. In the present investigation, miniature copper gears of 2 mm thickness are cut by WEDM and the machine parameters are optimized.

Keywords Addendum · Dedendum · Electron dispersive spectroscopy Gears · Pulse on time · Pulse off time · Single pitch error · Wire tension Wire feed rate

K. D. Mohapatra (✉) · S. K. Sahoo
Department of Mechanical Engineering, National Institute of Technology Rourkela, Rourkela, India
e-mail: kitu.kasinath1@gmail.com

S. K. Sahoo
e-mail: sks@nitrkl.ac.in

S. S. Pande and U. S. Dixit (eds.), *Precision Product-Process Design and Optimization*, Lecture Notes on Multidisciplinary Industrial Engineering,
https://doi.org/10.1007/978-981-10-8767-7_11

Nomenclature

D Pitch circle diameter
F Fisher's value
F_{pt} Single pitch error
F_p Theoretical pitch
h Workpiece thickness
K Diameter of the wire
l Length of cut
m Alternatives
N Number of teeth
n Objectives
P Probability value
P_d Diametric pitch
R^2 Regression coefficient
T_{on} Pulse on time
T_{off} Pulse off time
t Time between the cutting length
V_C Cutting speed
Wf Wire feed rate
W_i Weight of the criterion
Wt Wire tension
X_{ij} Response
Y_i Modified coefficient ratio

1 Introduction

Wire EDM or Wire Electric Discharge Machining process is an unconventional machining process used for cutting of different complex shapes of a conductive material. Till today, manufacturing industries face difficulties to design and cut intricate shapes using other conventional processes. Wire EDM makes it easier to cut different types of conductive materials making it much faster using altered parameter settings. The mechanism of the wire EDM is the involvement of vaporization and melting in which the materials are removed by thermoelectric erosion process by an electric spark created between a very thin wire (usually brass of diameter 0.25 mm) and an electrically conductive workpiece material. The wire in the spool is continuously fed to the workpiece to cut the material from the workpiece and the process occurs in an optimized speed such that there is a less chance of breakage in the wire. A high-frequency DC pulse power is used in the spark gap between the wire and the workpiece. This causes the existence of tiny sparks and the energy contained in it removes a fraction of workpiece material. The machine uses distilled water as a dielectric as it acts also as a coolant to the material and wire. Wire EDM is used for

cutting many complex geometries and 3D shapes which are difficult to machine by other conventional and non-conventional processes.

The present work deals with the cutting of small miniature gears made of copper with thickness 3 mm. The machining is carried out using brass wire as the tool electrode having a diameter of 0.25 mm and distilled water as the dielectric fluid. The experiment was carried out using four input parameters at two levels each repeated twice. Pulse on time, wire feed rate, pulse off time, and wire tension are taken as the process parameters and material removal rate and single pitch error were taken as the output parameters for the experiments. Totally 32 teeth have been obtained by conducting 32 sets of experiments, each parameter being machined considering two gear teeth. Totally four gears have been obtained each having 16 numbers of teeth and the responses, i.e. material removal rate and pitch error have been obtained and assessed from these experiments. A Multi-objective optimization technique using MOORA (Multi-objective Optimization using Ratio Analysis) method has been performed to know the optimum settings out of the 32 combinations obtained for the experiment. ANOVA (Analysis of Variance) table and response table has been obtained to know the significant process parameters affecting the output responses. The effects of response parameters on different process parameters have been analysed. Microstructural analysis has been carried out using SEM (Scanning Electron Microscope) for the wire (brass) and the workpiece (copper) to study and investigate the various defects, microstructures and surface characteristics of the cutting surface of the machined gear. Electron Dispersive Spectroscopy (EDS) was carried out to know the particular compound and composition present in the material. The optimum settings obtained for the gear can be used for manufacturing and production of large quality miniature gears.

2 Literature Review

Many works on WEDM, in general, gear cutting by WEDM in particular, have been carried out by the different researchers. On surface integrity of miniature spur gears by WEDM was carried out by Gupta and Jain (2014). They found that the combination of low discharge energy parameters leads to better accuracy and surface finish of the miniature gears. Gupta and Jain (2014) analysed and optimized the micro-geometry of miniature spur gears by wire EDM. Menz (2003) developed a 3D micro-structuring of ceramics and materials for high aspect ratio in micro-wire EDM process. The micro-geometry of miniature spur gears by wire EDM process were studied by Taylor et al. (2013). They suggested that in order to manufacture high-quality miniature gears, the use of pulse on time and voltage should be low. Yeh et al. (2013) studied the surface characteristics of polycrystalline silicon using phosphorous dielectric on wire electric discharge machining process. A multi-objective optimization was carried out for a 3D surface topography by Ming et al. (2014) in machining of YG 15 in WEDM. The spark erosion machining of miniature gears was studied by Gupta et al. (2015). Mandal et al. (2015)

modelled and optimized C-263 superalloy using multi-cut strategy in wire EDM. They used the desirability function for the prediction of the optimal settings. Habib and Okada (2015) studied the movement of the wire electrode in WEDM process. They found the backward deflection of the wire in fine WEDM process. Wentai et al. (2015) investigated the change in the wire tension in high-speed wire electric discharge machining. The wire tension was found to be capable enough to remain stable during the machining process. Kuriakose et al. (2003) studied the data mining applied to the wire EDM process. They conducted the experiments collected from the conducted data and they also tested it on additional data. They arrived at a conclusion that the model that was built using data mining provides good results with desired accuracy. With the improvement in the surface roughness, the material removal rate was a major concern for the wire EDM process. A development of the cylindrical wire EDM process, surface integrity and roundness was studied by Qu et al. (2002). The accuracy improvement in the wire EDM by real-time wire tension control was examined by Yan and Huang (2004). They attached dynamic absorbers to the idle rollers of wire transportation mechanism so that the vibration of wire tension is reduced during wire feeding. They concluded that with the attachment of the dynamic absorbers, small steady-state error and fast transient response can be obtained with geometrical contour error of corner cutting reduced to approximately 50%. Miller et al. (2004) investigated the spark cycle on material removal rate in wire EDM of advanced materials. They used metal bond diamond grinding wheels and porous metal foams in their experiment. They identified five types of constraints developed during machining, i.e. wire breakage, machine slide speed limit, MRR due to short circuit and pulse on time upper and lower limits. Further the capability of WEDM process was also established by them to machine different advanced materials. In the meantime, several researchers tested the wire EDM parameters. Liao et al. (2004) conducted Analysis of Variance (ANOVA) and *Fischer* test (*F*-test) in order to obtain a fine surface finish in wire EDM. They found that low conductivity of dielectric should be amalgamated for the discharge spark to take place with the best surface finish of 0.22 μm. They further concluded that the traditional circuit should be modified using low power for ignition in order to achieve a good surface roughness during machining. The cutting parameters were still a major concern when Kanlayasiri and Boonmung (2007) investigated the effects of wire EDM machining parameters on surface roughness of newly developed DC53 die steel. They investigated on the machining parameters such as pulse on time, pulse off time, wire tension and pulse peak current. Further they employed quantitative testing methods in place of qualitative testing techniques on residual analysis. Their findings concludes that based on ANOVA, pulse peak current and pulse on time were the significant variables to affect the surface roughness of wire-EDMed DC53 die steel. As the wire deforms resulting in the deviations in the inclination angle of machined parts, Plaza et al. (2009) developed some original models for the prediction of angular error in WEDM taper cutting. The two original models were developed by them for the prediction of angular error to decrease the experimental load and contribute a general approach to the problem. Their findings showed that the taper angle and the part thickness were the most influencing

variables in the problem. The angular error in wire EDM taper cutting was studied by Sanchez et al. (2008) when he designed a new approach to the prediction of angular error in taper cutting. They derived a quadratic equation for the prediction of angular error in taper cutting. They reported that the influence of the angular error is mostly due to the angle and the part thickness determining wire's mechanical behaviour. Soon with the advancement of the taper cutting, the corner cutting were also given importance and hence the corner cutting accuracy of thin parts using wire electric discharge machining was carried out by Dodun et al. (2009). Their results disclosed that the outside corners can be obtained with a small thickness and corner angle having the shape of post-yield bending when accompanied by the machining error. Yan and Liu (2009) designed, analysed and experimented the study of a high-frequency power supply for finish cut of wire EDM. They developed a high-frequency power supply for the improvement of surface quality in wire EDM. Their findings revealed that the electrolytic effect of tungsten carbide can be reduced by pulse duration ratio in a high discharge frequency of more than 500 kHz.

From the literature review, it was observed that very few works have been carried out in gear cutting of copper by wire EDM process. In view of it, the objective of the present work is to focus on producing spur gears made of copper, to maximize the MRR and minimize the error present in the gears by optimizing the responses and to obtain a best combination from the present settings so that the time can be reduced. In addition to it, the machining of copper gear by wire EDM process at the obtained optimized setting will be an advantage in producing copper gears by achieving faster machining rate.

As the machining of gears by copper have an application in various transportation oils such as diesel, petroleum, semiconductor industries, lubricant oils, clocks, radiators, aerospace, printing, papermaking, mining industries, electric motors, trucks, air brakes, etc., the obtained optimized setting can be an advantage over other combinational settings to produce high-quality miniature spur gears made of copper.

3 Experimental Setup

3.1 Machines, Materials and Specifications

The experimental work is carried out using an ELECTRONICA EPULSE 15® machine. As copper gears have important applications in many industries mentioned above, so copper was chosen as the workpiece material of thickness 3 mm. A brass wire of diameter 0.25 mm is taken as the tool electrode for the machining operation. Distilled water is used as the dielectric fluid for carrying out the present work. Figure 1 displays the schematic diagram of wire EDM process. The composition of the brass wire is a pure brass of 65% copper and 35% of zinc. The machine uses a high-voltage DC servo stabilizer of 400 V.

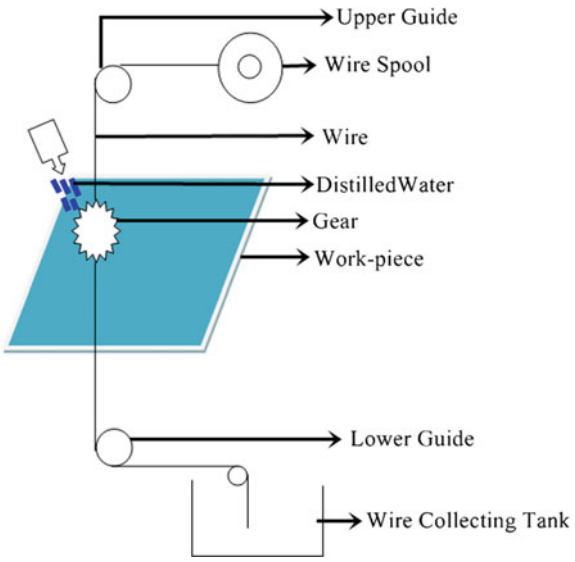

Fig. 1 Schematic diagram of wire EDM process

3.2 *Parameter Settings and Gear Specifications*

The machine parameters are chosen according to the machine restraints and past literature survey. To conduct the experiment, four input parameters were chosen at two different levels repeated twice. The combinations were obtained from Minitab 16® software with 32 numbers of setting combinations. Pulse on time (T_{on}), pulse off time (T_{off}), wire tension (Wt) and wire feed rate (Wf) were taken as the process parameters.

The other wire EDM parameters such as peak current, servo voltage, peak voltage, water pressure and servo feed rate were kept constant for the experiment. The response parameters such as Material removal rate and single pitch error (SPE) were obtained after the machining operation.

The model of the gear is constructed using ELCAM® software giving necessary geometric parameters. The gear model was designed giving required pressure angle of 20°, pitch circle diameter (D) of 10 mm and number of teeth (N) as 16. Table 1 depicts the parameters and range considered for conducting the experiment.

Table 1 Parameters and range considered for the experiment

Input parameters	Units	Symbol	Levels	
			I	II
Pulse on time	µs	Ton	105	110
Pulse off time	µs	Toff	53	58
Wire feed rate	m/min	Wf	3	5
Wire tension	Kg-f	Wt	5	7

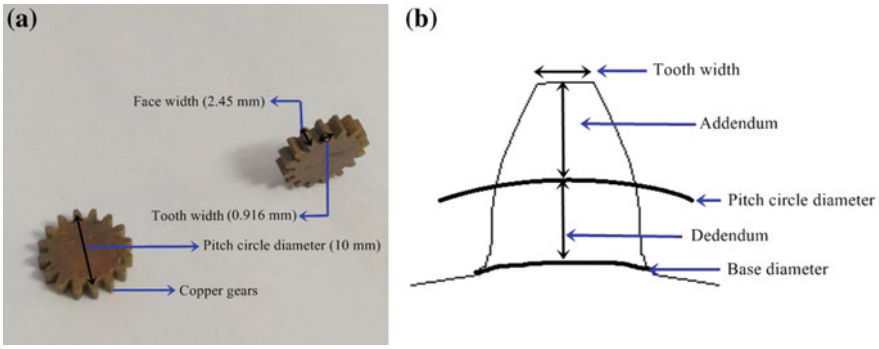

Fig. 2 Gears obtained after the machining operations **a** specifications of the gear and **b** gear terminologies

Figure 2 shows the different gears obtained after the machining operation, its specifications and terminologies. The experiment was carried out for all the 32 sets of the combinations considering each two teeth's as one set. So an all total of 4 gears were obtained having sixteen numbers of teeth on one gear. So in one gear eight sets of combinations were carried out. The gears obtained were measured for calculating the single pitch error produced in the teeth. Table 2 depicts the specification of gears obtained for the machining process.

3.3 Calculation of the Response Parameters

The response parameters obtained were measured for the experimental investigation and analysis. The material removal rate is obtained by taking the cutting speed, wire diameter and workpiece thickness into consideration. Cutting speed is calculated by taking length and time into consideration. Higher the pulse on time, more is the removal of material. The *material removal rate* (mm^3/min) is calculated by the following formula:

$$\text{MRR} = V_C \times h \times k, \tag{1}$$

Table 2 Gear specifications obtained for the machining operation

Material	Copper
Profile	Involute
Pressure angle	20°
Number of teeth	16
Pitch circle diameter	10 mm
Face width	2.45 mm
Tooth width	0.916 mm

where V_c is the cutting speed in mm/min, K is the diameter of the wire (0.25 mm) and h is the workpiece thickness (3 mm).

Similarly, the *cutting speed* is calculated by the following formula:

$$V_C = 60 \times l/t \text{ mm/min}, \tag{2}$$

where l is the cut length of two teeth's of the gear in mm and t is the time between the cutting length.

The machining time was calculated by using stopwatch from the starting point of the one tooth to the ending point of the same tooth for one gear tooth.

During the machining of the gears by wire EDM, some deviations occur while cutting of the gear tooth. These are nothing but the type of errors produced in the gear tooth during the machining operation. These errors arise due to noise and certain environmental condition during machining. Single pitch error is one of the pitch deviation error occurs during the machining of the gear tooth.

Single pitch error is calculated by taking two teeth into consideration. It is the difference between the theoretical and actual measured values of a pitch for a given pair of teeth or the deviation between the actual measured pitch values between any two adjacent tooth surfaces and the theoretical circular pitch.

$$\text{Single pitch error } (F_{\text{Pt}}) = \text{Theoretical Circular Pitch} - \text{Actual measured pitch values} \tag{3}$$

The actual measured values of pitch were obtained after the machining by taking the average of the two left flanks and right flanks distance into consideration.

The *theoretical circular pitch* (F_P) is calculated by the following formula:

$$F_p = \pi/P_d = \pi D/N, \tag{4}$$

where D is the pitch circle diameter in mm (10 mm), N is the number of teeth and P_d is the diametric Pitch.

Figure 3 depicts the image scale legend for 20× magnification zoom, where magnification 20× corresponds to 14.537 μm for 0.5 mm length. Similarly, the measurement of single pitch error for one combination (L_{21}) out of 27 combinations is depicted in Fig. 4. The measurement of single pitch error in Fig. 4 is measured in microns. The micron is then converted to millimetre according to the 20× scale.

The readings for the single pitch error were measured by using suitable software Caliper pro 4.2. From the Fig. 4a, A to B signifies the measurement of left flank and right flank for one gear tooth. A to a signifies the measurement of left flank measured from the software. Similarly, b to B signifies the measurement of right flank measured from the software. The readings were assessed and averaged thrice for the measurement and the average of the left flank and right flank were calculated for the measurement of the pitch error.

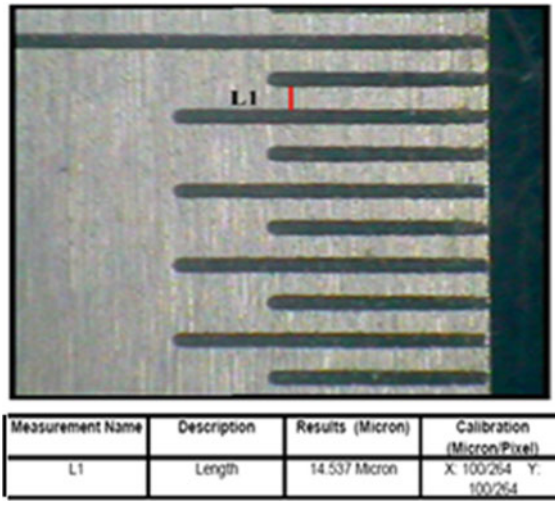

Fig. 3 Image scale legend while measuring the single pitch error at 20× magnification zoom

4 Multi-objective Optimization Using MOORA

The experiment was conducted for all the 32 sets of combinations. The output parameters, i.e. MRR and single pitch error were optimized using ratio analysis and is called multi-objective optimization using ratio analysis (MOORA). This method was first introduced by Brauer (2007), in order to solve various conflicting decision-making problems. The multi-objective response parameters are converted to single-objective response parameters by this method. In the present work, the MRR should be maximized and the single pitch error should be minimized. The decision matrix showing the performance of different alternatives can be written in the form:

$$X = \begin{bmatrix} X_{11} & \cdots & X_{12} & \cdots & X_{1n} \\ X_{21} & \cdots & X_{22} & \cdots & X_{2n} \\ \cdots & \cdots & \cdots & \cdots & \cdots \\ X_{m1} & \cdots & X_{m2} & \cdots & X_{mn} \end{bmatrix} \tag{5}$$

The method starts with a matrix of responses of different alternatives to different objectives:

$$\left(X_{ij}\right)_{\mathrm{MRR}} \text{ and } \left(X_{ij}\right)F_{\mathrm{pt}} \tag{6}$$

where X_{ij} is the response of the ith objective to the jth alternative, $i = 1, 2, \ldots, n$ are the objectives, $j = 1, 2, \ldots, m$ are the alternatives.

To achieve the problem, normalization is done so that the values transforms into a dimensionless number [0, 1].

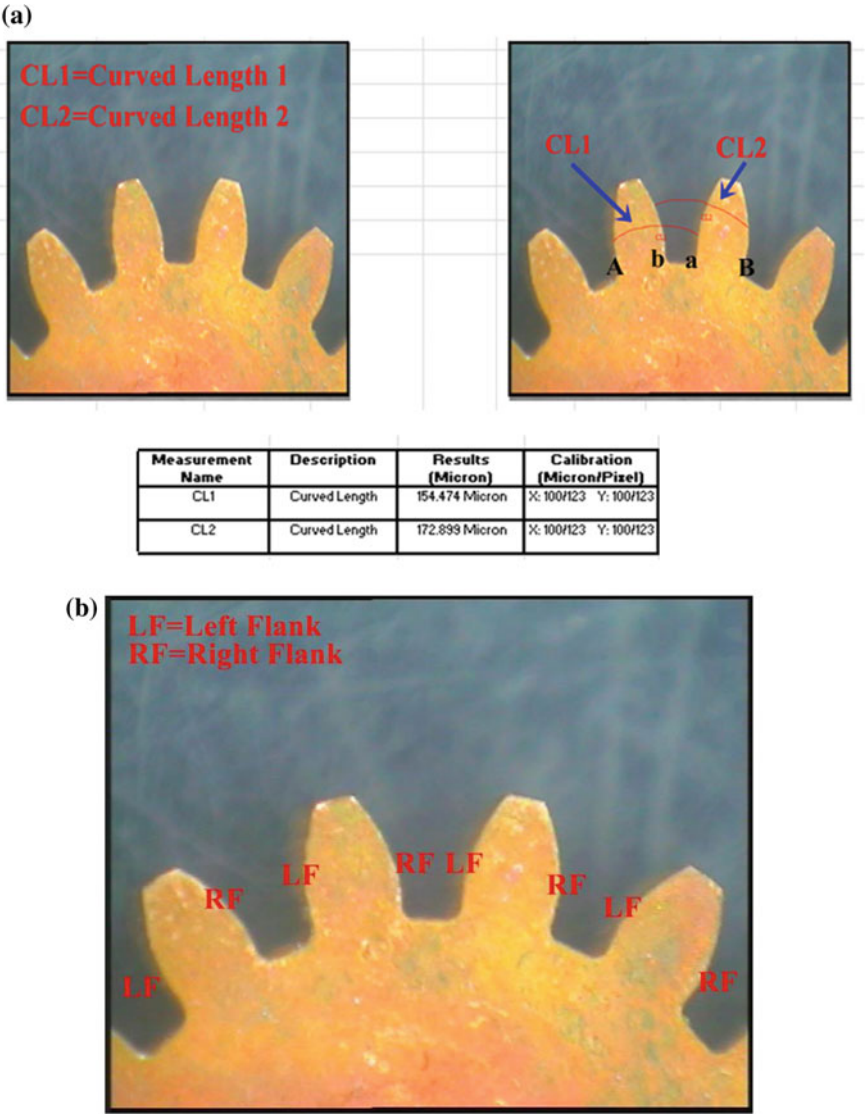

Measurement Name	Description	Results (Micron)	Calibration (Micron/Pixel)
CL1	Curved Length	154.474 Micron	X: 100/123 Y: 100/123
CL2	Curved Length	172.899 Micron	X: 100/123 Y: 100/123

Fig. 4 Measurement of single pitch error at 20× magnification zoom

The summation for MRR and F_{pt} were calculated as follows:

$$(X_{ij})_{MRR} = \sqrt{\sum_{i=1}^{m} X_{ij}^2} \text{ and } (X_{ij})F_{pt} = \sqrt{\sum_{i=1}^{n} X_{ij}^2}. \quad (7)$$

Step 1: The normalized decision matrix by vector method is calculated by the formula:

$$X_{ij,\mathrm{MRR},F\mathrm{pt}} = \frac{X_{ij}}{\sqrt{\sum_{i=1}^{m} X_{ij}^2}}, \quad i = 1, \ldots, n; j = 1, \ldots, m. \tag{8}$$

The MOORA method has two different components, ratio system and reference point approach. The responses are added in case maximization (MRR) and subtracted in case of minimization (single pitch error) for optimization.

Step 2: The ranking value according to ratio system is as follows:

$$Y_i = \sum_{i=1}^{g} X_{ij}^* - \sum_{i=g+1}^{n} X_{ij}^*, \tag{9}$$

where $\sum_{i=1}^{g} X_{ij}^*$ and $\sum_{i=g+1}^{g} X_{ij}^*$ are for the benefits and non-benefits criteria respectively.

$i = 1, 2, \ldots, g$ are the objectives to be maximized and $i = g+1, g + 2, \ldots, n$ are the objectives to be minimized and Y_i is the normal assessment of the alternative j with respect to all objectives.

If there are some attributes more important than others then the Ranking value becomes

$$Y_i = \sum_{i=1}^{g} W_i X_{ij}^* - \sum_{i=g+1}^{n} W_i X_{ij}^* \tag{10}$$

where W_i is the weight of the ith criterion.

Step 3: The Y_i values are ranked and the alternative with the highest value is chosen as the best alternative.

Step 4: The modified coefficient ratio is given by the following formula:

$$Y_i = \sum_{i=1}^{g} X_{ij}^* / \sum_{i=g+1}^{n} X_{ij}^*. \tag{11}$$

Table 3 depicts the experimental design values of both input and output parameters obtained by using L_{32} orthogonal array and the optimization was carried out by combining the output responses using Ratio analysis. The multi-objective responses, i.e. MRR and single pitch error were optimized to single-objective response MCR (Modified Coefficient Ratio) using ratio analysis. From the above table, the highest coefficient rank corresponds to the 24th setting of the combinations which is considered as the best alternative. So T_{on} 110-T_{off} 53-Wf 5-Wt 7 is chosen the best combination of the gear made of copper to be manufactured in the field of wire EDM within these settings.

Table 3 MOORA Optimization of L32 orthogonal array

S. No.	Input parameters				Output parameter		MOORA	
	T_{on}	T_{off}	Wf	Wt	MRR	F_{Pt}	MOORA coefficient	rank
1	105	53	3	5	1.26	1.2	0.6841	24
2	105	53	3	5	1.24	1.08	0.7510	18
3	105	53	3	7	1.31	1.14	0.7498	19
4	105	53	3	7	1.30	1.18	0.7205	21
5	105	53	5	5	1.34	1.22	0.7182	22
6	105	53	5	5	1.37	1.22	0.7343	20
7	105	53	5	7	1.35	1.13	0.7783	17
8	105	53	5	7	1.23	1.16	0.6947	23
9	105	58	3	5	1.04	1.09	0.6228	25
10	105	58	3	5	1.08	1.25	0.5629	32
11	105	58	3	7	1.06	1.16	0.5981	30
12	105	58	3	7	1.10	1.14	0.6298	26
13	105	58	5	5	1.04	1.12	0.6018	28
14	105	58	5	5	1.03	1.12	0.6004	27
15	105	58	5	7	1.05	1.15	0.5948	29
16	105	58	5	7	1.02	1.14	0.5788	31
17	110	53	3	5	2.25	1.07	1.3700	3
18	110	53	3	5	2.10	1.06	1.2914	8
19	110	53	3	7	2.13	1.02	1.3650	5
20	110	53	3	7	2.23	1.08	1.3452	4
21	110	53	5	5	2.35	1.11	1.3793	2
22	110	53	5	5	2.26	1.21	1.2125	12
23	110	53	5	7	2.06	1.14	1.1784	15
24	*110*	*53*	*5*	*7*	*2.18*	*1.03*	*1.3802*	*1*
25	110	58	3	5	2.09	1.04	1.2993	7
26	110	58	3	5	2.03	1.06	1.2489	10
27	110	58	3	7	2.08	1.11	1.2172	14
28	110	58	3	7	2.02	1.05	1.2493	11
29	110	58	5	5	1.87	1.09	1.1125	16
30	110	58	5	5	2.28	1.15	1.2839	6
31	110	58	5	7	2.09	1.08	1.2620	9
32	110	58	5	7	1.98	1.04	1.2341	13

5 Analysis of the Experiment

5.1 Microstructural Study of Material and the Wire

The objective of carrying out the material analysis is to investigate and analyse the various surface defects of the copper plate material at the optimized settings obtained from the wire EDM parameters. The surface metallography needs to be investigated as wire EDM is a thermal dominant process and the very high temperature has a significant impact on the process-induced surface integrity including microstructure change, surface characteristics and grain structure.

The experiment was conducted and the output parameters, i.e. MRR and single pitch error were optimized using MOORA method to get the best alternative. The material and the wire with the best alternative T_{on} 110 µs, T_{off} 53 µs, Wf 5 m/min and Wt 7 kg-f are now analysed for the various qualitative and microstructural analyses of the study.

5.1.1 Study of Grain Structure

The optimized setting of the teeth was first seen under the optical microscope and then the image is viewed under scanning electron microscope to know the presence of grains after etching. In order to see the grain structure, proper etchant should be applied to the machined gear tooth. The etchant used for copper is distilled water (50 ml) and Nitric acid (50 ml).

Figure 5a, b depicts the optical image of the gear visualized at the surface at 400× zoom and Fig. 5c depicts the SEM image of the gear at 300× zoom after the etchant has been applied. From the figures, it can be observed that some grains like structures or grain boundaries are formed on the machined material surface after etching. The formations of grains are due to the structure, composition or phase of the metal that creates electrochemical potentials when exposed to an etchant.

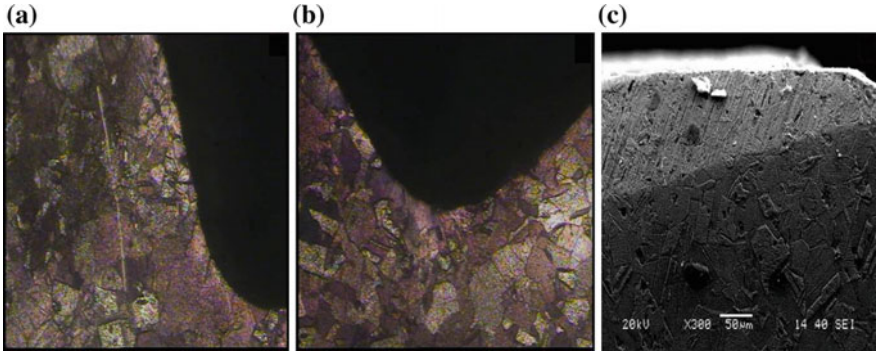

Fig. 5 Optical and SEM image of the copper at 400× and 300× zoom

5.1.2 Study of Surface Characteristics Using Scanning Electron Microscope (SEM)

The gear tooth is placed under scanning electron microscope and the micrographs were studied for both the material and the brass wire. Figure 6 describes the SEM image of the workpiece material at 10,000× zoom. It can be observed that there are some voids and cracks formation on the surface of the workpiece material. Some dark regions spots such as pores were clearly visible on the work material. High-speed spark energy density and wire feed rate were the reasons for the occurrence of such voids and cracks due to the sparks generated from the wire. It is clear that the surface characteristic of the WED machined surface depends upon the applied discharge energy.

Figure 7 depicts the SEM analysis of the copper material at 5000× and 50,000× magnification zoom. From the Fig. 7a, it can be observed that some holes and heat-affected zone (HAZ) were formed on the material surface. The heat-affected zone is associated with grain growth, high tensile residual stress, porosity, and dielectric fluid. The formation of the hole is due to the high discharge energy of the spark with a high spark on time. The heat-affected zone formation is due to the change in temperature, rapid heating, continuous high sparks and quenching in the WEDM process. The bull eye was also marked as shown in Fig. 7a and the occurrence of bull eye is due to the presence of oxygen-rich layer. A lump of debris was also identified at high discharge energy settings as depicted in Fig. 7b. The dielectric carries out some of the molten material at high discharge energy settings. The leftover molten material re-solidifies to form lumps of debris.

Figure 8 depicts the SEM analysis of the copper material at 10,000× magnification zoom. Pores and holes were formed on the material surface as shown in Fig. 8a. The pores are formed due to the frequent melting expulsion on the wire

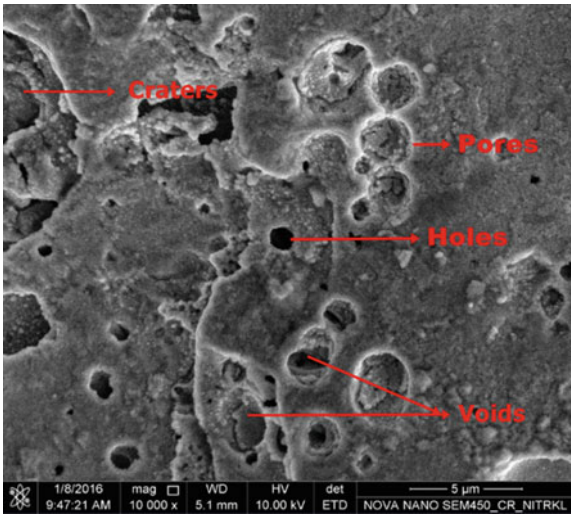

Fig. 6 Micrographs of the copper material at 10,000× zoom

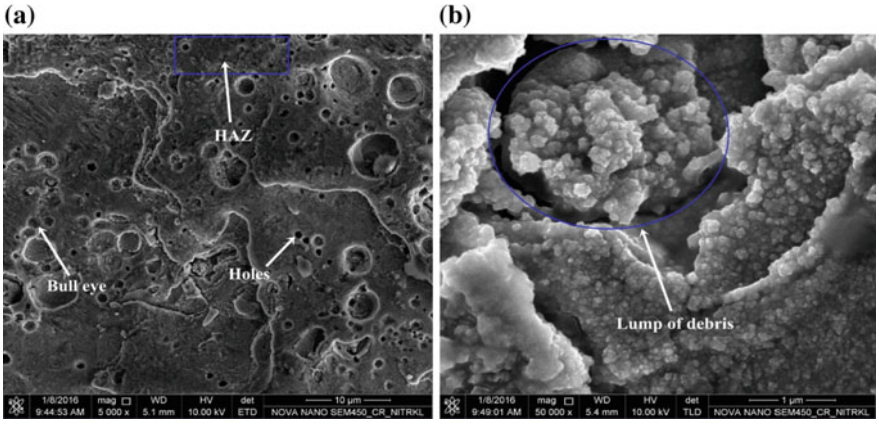

Fig. 7 SEM analysis of the copper material at **a** 5000× and **b** 50,000× magnification zoom

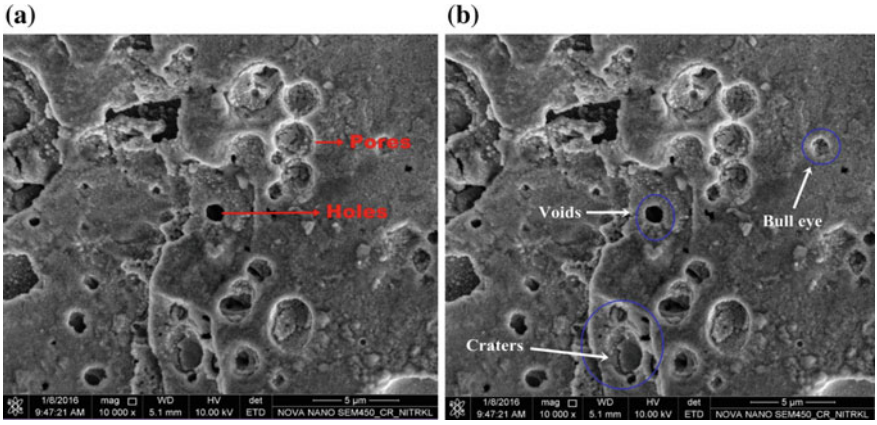

Fig. 8 SEM analyses of the copper material at 10,000× magnification zoom

surface due to high pulse on time. High spark energy density at high wire feed rate causes the material to form surface holes during machining operation. Similarly, Fig. 8b shows voids and craters due to high spark energy density at high pulse on time causing the sparks to create such formations on the material surface.

Figure 9 depicts the SEM analysis of the copper material at 20,000× magnification zoom. Craters and voids were visible on the material surface as displayed in Fig. 9. The violent sparks with high-energy density and the various forces occurring in the wire lag lead to the formation of voids and craters on the material surface. Similarly, the melted debris was identified on the material surface as shown in Fig. 9b due to the deposition of the melted material formed due to the solidification of the spark at high discharge energy settings. The high discharge energy of the

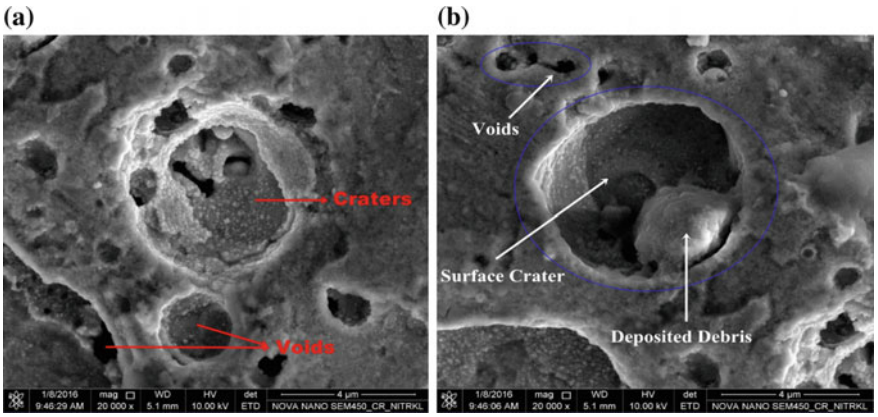

Fig. 9 SEM analyses of the copper material at 20,000× magnification zoom

plasma channel results in melting of the material but it is not sufficient to produce a high exploding pressure which can spray all the molten metal away from the machined surface. The gas bubbles banish from the molten material when the remaining molten material solidifies on the surface resulting in micro-voids.

Figure 10 depicts the microstructural analysis carried out for the wire at the optimized setting of the response T_{on} 110 µs, T_{off} 53 µs, Wf 5 m/min, and Wt 7 kg-f. Figure 10a displays the affected damaged zone indicating that the wire is being affected by the sparks produced from the wire at high discharge rate. Some cracks and melted deposits were also marked over the wire surface as shown in Fig. 10b. High discharge energy at high servo voltage and wire feed rate results in the formation of such cracks. Moreover high peak current and induced stresses exceeding the wires ultimate tensile strength are the reasons for the formation of cracks.

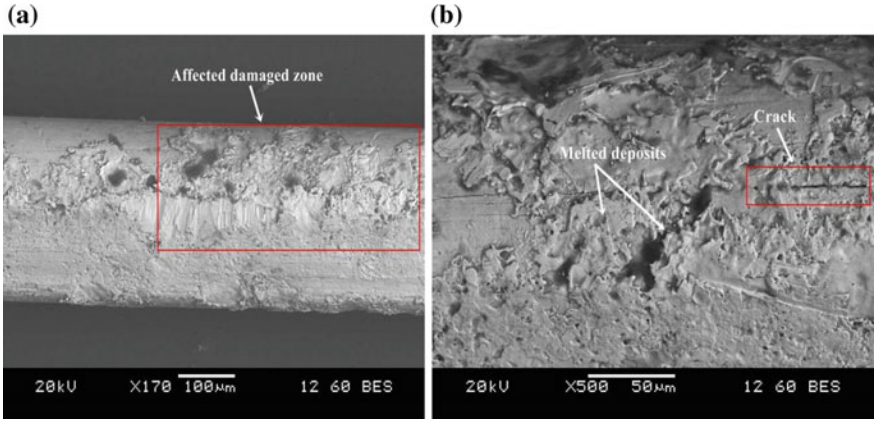

Fig. 10 Microstructural analysis of the wire

5.2 Elemental Analysis

The very high temperatures of the sparks (up to 45,000 K) subsequently melt and vaporize the surface of the workpiece material during the discharge process. As a result complex chemical reactions take place between wire material, workpiece material, and the dielectric. The analysis is measured by using EDS so that the element composition of the machined surfaces and wires can be analysed.

5.2.1 EDS of Copper Material

EDS or Energy-Dispersive X-ray Spectroscopy is used for analysing chemical characteristics of the material.

The EDS of the copper plate is shown in Table 4.

The elements present on the workpiece material are indicated by the peaks corresponding to their energy levels. The weight percentage of the carbon was found to be 20.68 and that of the copper was found to be 79.32% in the *K*th shell. The EDS of the copper material is shown in Fig. 11. The presence of carbon and oxygen are negligible due to significantly reduced discharged energy.

5.2.2 EDS of Brass Wire

The EDS analysis of the brass wire electrode at the optimized settings (T_{on} 110 µs, T_{off} 53 µs, Wf 5 m/min and Wt 7 kg-f) was exposed at high discharge energy settings to know the presence of foreign elements such as Cu, O, and Zn on the WED machined surface migrated in considerable quantities. Figure 12 depicts the EDS analysis of brass wire electrode.

The section of the machined wire surface scanned was subjected to EDS and the weight % and atomic % of the elements formed was analysed. Table 5 shows the EDS analysis of brass wire electrode. It was concluded that the elements present in the brass wire after machining were Cu and Zn with the weight % of Cu as 54.66% in the *L*th shell and Zn as 45.34% in the *L*th shell. The presence of copper was detected due to the diffusion of the material between the brass wire electrode to the workpiece material.

Table 4 EDS of the copper material

Element	Weight %	Atomic %
C K	20.68	57.99
Cu K	79.32	42.01
Total	100	

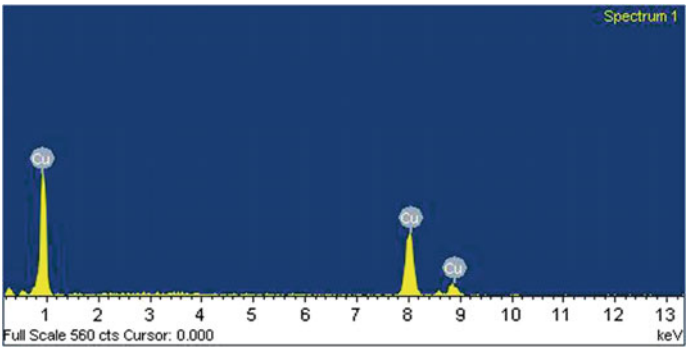

Fig. 11 EDS of the copper material

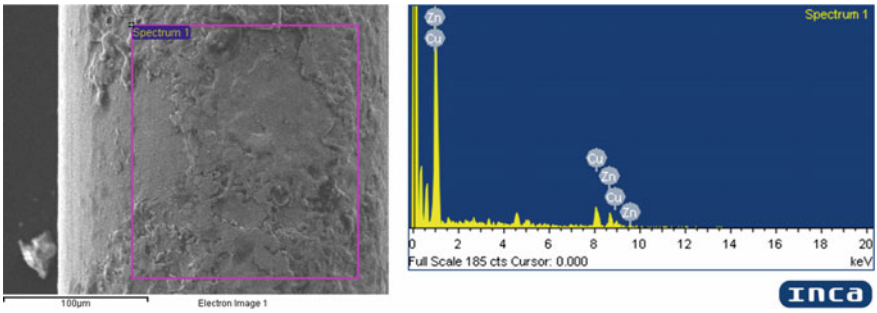

Fig. 12 EDS of brass wire electrode

Table 5 EDS analysis of brass wire electrode

Element	Weight %	Atomic %
Cu L	54.66	55.36
Zn L	45.34	44.64
Total	100	

6 Results and Discussion

6.1 ANOVA Table for Means

Table 6 shows ANOVA for the means. The factors affecting the response can be determined by the ANOVA table.

If the probability (P) value <0.05, the factor is said to be significant. From Table 6, it was observed that pulse on time and pulse off time are the most crucial factors contributing the most in the prediction of the output responses. The R-Square also corresponds to 97.52% of the total value for the experiment.

Table 6 ANOVA table for means

Source	DF	SS	MS	F (Fisher's)	*P*
T_{on}	1	3.006	3.006	1031.5	0.000
T_{off}	1	0.085	0.085	29.41	0.000
Wf	1	0.004	0.004	1.40	0.248
Wt	1	0.0003	0.0003	0.11	0.739
Error	27	0.078	0.0029		
Total	31	3.175			

Table 7 Response table for means

Level	T_{on}	T_{off}	Wf	Wt
1	0.6638	1.0221	0.9816	0.9671
2	1.2769	0.9186	0.9591	0.9736
Delta	0.6131	0.1035	0.0226	0.0064
Rank	1	2	3	4

6.2 Response Table for Means

The rank of the process parameters are determined by the response table. The response table of the process parameters is shown in Table 7.

From the response table, it was analysed that the pulse on time is the most determining parameter followed by pulse off time, wire feed rate and wire tension.

6.3 Statistical Models for MRR and Single Pitch Error

Kanlayasiri and Boonmung (2007) suggested some multiple linear regression models that are suitable in predicting various performance measures in wire EDM process. The regression equations of the statistical models of the responses were obtained by using suitable software by selecting the input and output responses of the model. The experimental results were obtained after the gear has been machined by wire EDM process. Regression coefficient (R^2) 0.975 and 0.942 in MRR and pitch error, respectively, indicates a good sign of statistical model values with the experimental. The statistical regression models for MRR and single Pitch error can be given by the following equations:

$$\text{MRR} = -16.5 + 0.190 * T_{on} - 0.0389 * T_{off} + 0.0056 * \text{Wf} - 0.0136 * \text{Wt} \quad (12)$$

$$\text{and } F_{Pt} = 2.79 - 0.0141 * T_{on} - 0.00258 * T_{off} + 0.0127 * \text{Wf} - 0.0111 * \text{Wt}. \quad (13)$$

Figure 13 displays the comparison between statistical and experimental model values of MRR. Similarly, the comparison between the statistical and the experimental values for single pitch error is displayed in Fig. 14. Both the graph confirms a good agreement of the results between the statistical and the experimental model values.

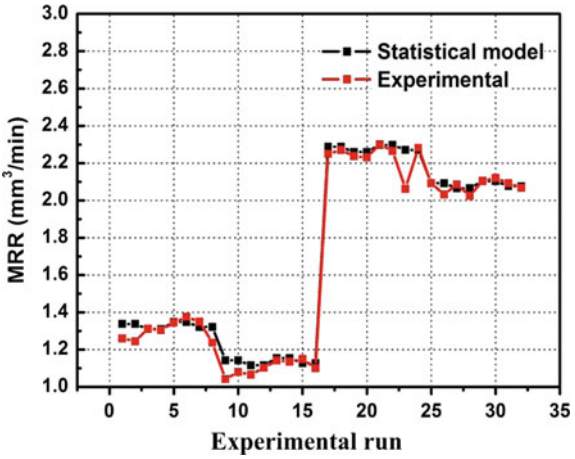

Fig. 13 Comparison between statistical and experimental values of MRR

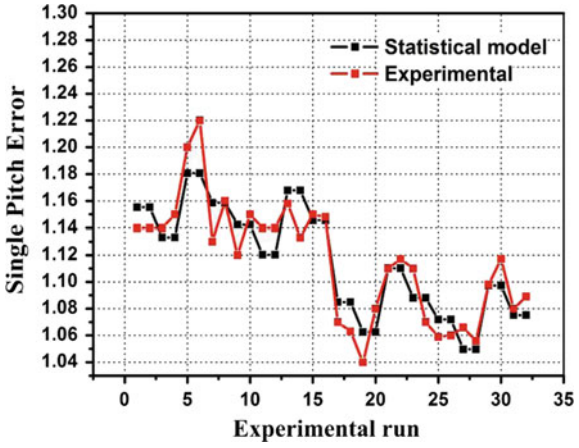

Fig. 14 Comparison between statistical and experimental values of single pitch error

6.4 *Various Plots Obtained During Analysis*

6.4.1 Main Effect Plot

Figure 15 depicts the main effect plot diagram for the modified coefficient ratio (MCR). Figure 15 depicts the main effect plot diagram for the modified coefficient ratio (MCR). The MRR should be maximized so that the cutting speed and the machining rate should be higher while machining of the materials. Similarly, the errors in the pitch should be lower or in other words, the single pitch error should be minimized. The obtained MCR after optimizing the multi-objective responses should be considered as highest the better and the combinations for the best alternative can be evaluated by ordering their ranks. The mean for each input factors with respect to the MCR was analysed and is depicted in Fig. 15. From the Fig. 15a, the MCR increases with the increase in the pulse on time. The modified coefficient ratio has the highest impact on pulse on time 110 µs rather than pulse on time 105 µs. High values of pulse on time results in high discharge energy of the spark which further results in higher values of MCR.

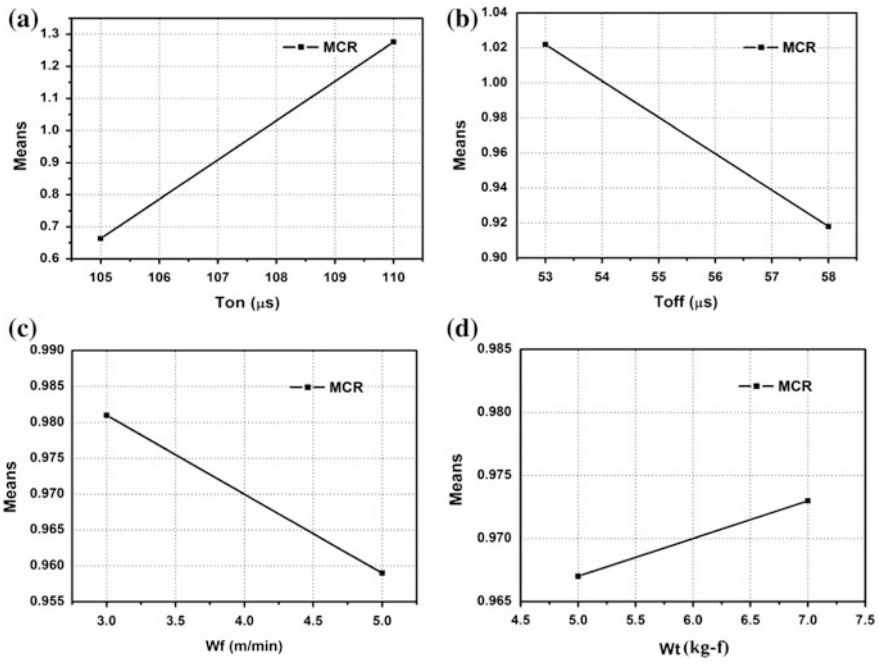

Fig. 15 Main effect plot for modified coefficient ratio

Similarly from the Fig. 15b, the MCR decreases with the increase in the pulse off time. With the increase in the wire feed rate, the MCR decreases as shown in Fig. 15c. Similarly the MCR increases with the increase in the wire tension as the discharge energy drawn from the wire is more at low wire feed rate and is shown in Fig. 15d.

6.4.2 Surface and Contour Plots

Surface plots and contour plots are designed to express the potential relationship between the input and output variables. The contour plot is a substitute of 3D surface plot. The contour plot and surface plots can hold two continuous factors at a time. The contour plots can be represented in terms of area, contour lines and area and contour lines.

Figure 16 depicts the 3D surface plot analysed for the MCR with respect to the input variables. The region with the darkest colour indicates highest MCR while the region with the lightest colour indicates lowest MCR. Figure 16a depicts the 3D surface plot of MCR versus T_{on} and T_{off}. From Fig. 16a, it can be concluded that the highest MCR corresponds to T_{on} 107 µs and T_{off} 53 µs. Figure 16b depicts the 3D surface plot of MCR versus T_{on} and Wt. Similarly from Fig. 16b, it can be resolved that the highest MCR corresponds to Wt 5 kg-f and T_{on} 110 µs.

Figure 17 depicts the contour of MCR versus T_{on} and T_{off} of areas only. The contour plot displays a stationary ridge topographical map with the rows increasing in a uniform manner. The darkest region corresponds to highest MCR (>1.35) which reveals that the MCR is highest in the region of T_{on} 110 µs and T_{off} 53 µs. With the increase in the pulse off time, the MCR goes on decreasing in between the range of T_{on} 109–110 µs. This indicates that a higher material removal rate and lower single pitch error can be achieved at low values of pulse off time and high values of pulse on time.

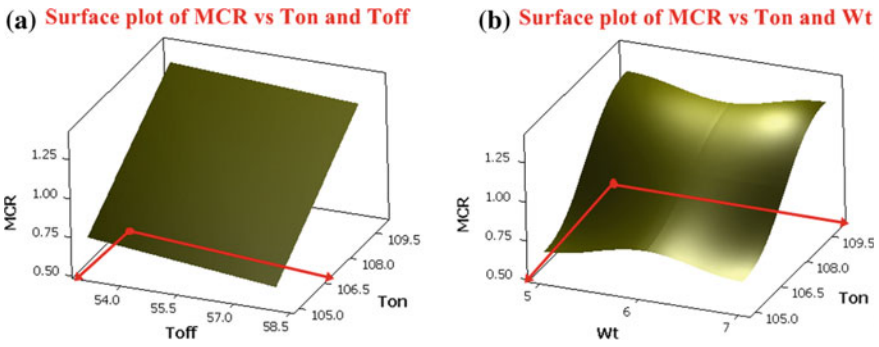

Fig. 16 3D surface plot for modified coefficient ratio

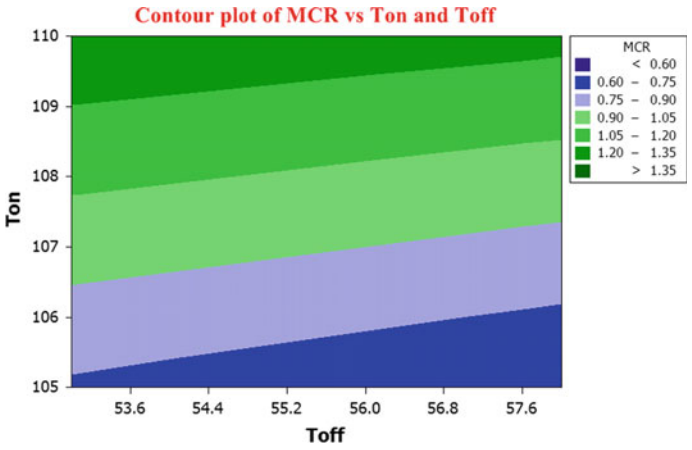

Fig. 17 Contour plot for modified coefficient ratio

6.5 Effects of Response Parameters on Process Parameters

6.5.1 Effect of Material Removal Rate

Figure 18 depicts the effect of MRR on process parameters. Figure 18a depicts the effect of MRR at increasing pulse on time and pulse off time at constant wire feed rate and wire tension. With the increase in the pulse on time at increased pulse off time, the MRR tends to increase. With the further increase in the wire tension at constant wire feed rate, the MRR increases as shown in Fig. 18b. The increase in the MRR is due to the high pulse on time at high discharge energy settings causing the spark intensity to increase thereby increasing the cutting speed and machining rate. With the further increase in the wire feed rate, the MRR also increases as shown in Fig. 18c. This is due to the fact that at high pulse on time and due to higher wire feed rate, the cutting time is reduced with the occurrence of high sparks thus increasing the material removal rate. With the further increase in the wire tension (Fig. 18d), the MRR increases due to the high reaction forces cause the spark to create more heat and temperature thereby increasing the machining rate and cutting speed.

6.5.2 Effect of Single Pitch Error

Figure 19 depicts the effect of single pitch error on process parameters. Figure 19a depicts the effect of single pitch error at increasing pulse on time and pulse off time at constant wire feed rate and wire tension. There is a decrease in the single pitch error as depicted from Fig. 19a. High discharge energy at low wire feed rate and wire tension result in uniform machining of the gear tooth without any deviation.

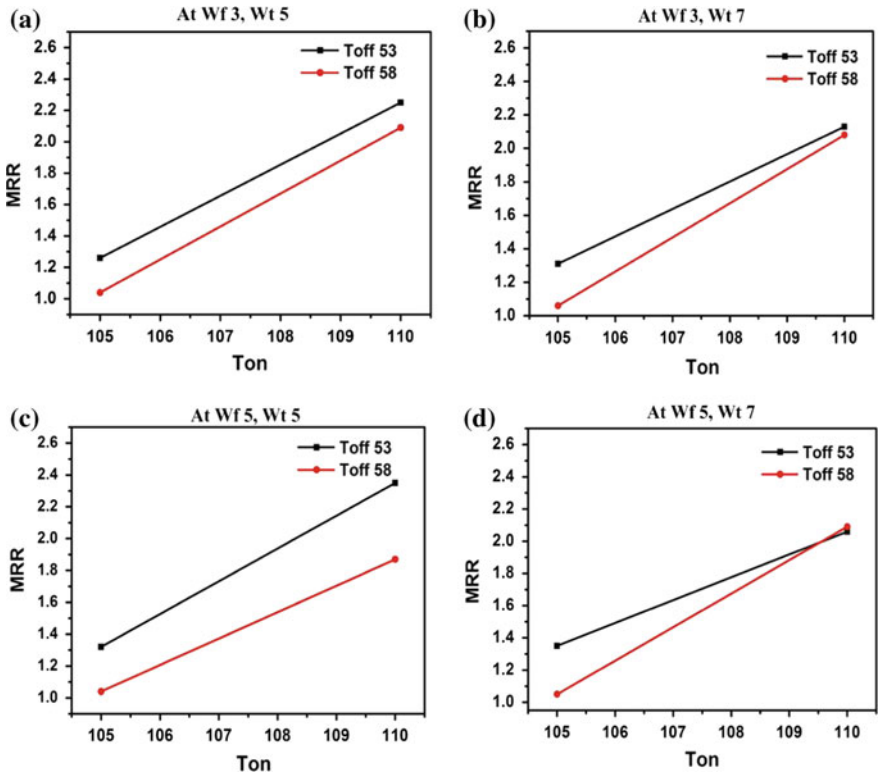

Fig. 18 Effect of MRR on process parameters

With the further increase in the wire tension at low wire feed rate, the wire is stretched more tightly in between the upper and lower guide providing uniform cutting of the gear tooth with little/no deviations. Hence, the error tends to minimize or decrease (1.17) even if the pulse on time is increased as displayed in Fig. 19b. The sparks produced from the wire remains unchanged at high discharge energy and high pulse off time at low wire feed rate. With the increase in the wire feed rate (Fig. 19c) and at low pulse off time (53 μs), the error slightly increases (1.21) due to the rapid movement of the wire resulting in the irregular cutting of the gear profile at high discharge settings. With the further increase in the wire tension (Fig. 19d), at high discharge energy and low pulse off time, the pitch error tends to increases. The increase in the pitch error is due to the fact that at high discharge energy, wire feed rate and wire tension the occurrence of the spark is more but due to the low pulse off time (53 μs), the spark termination time and voltage for the gap is reduced for the period and this results in the plasma channel to draw more discharge energy from the wire resulting in an increase in the spark efficiency thus leading to irregularity of the gear tooth and deviations in the profile.

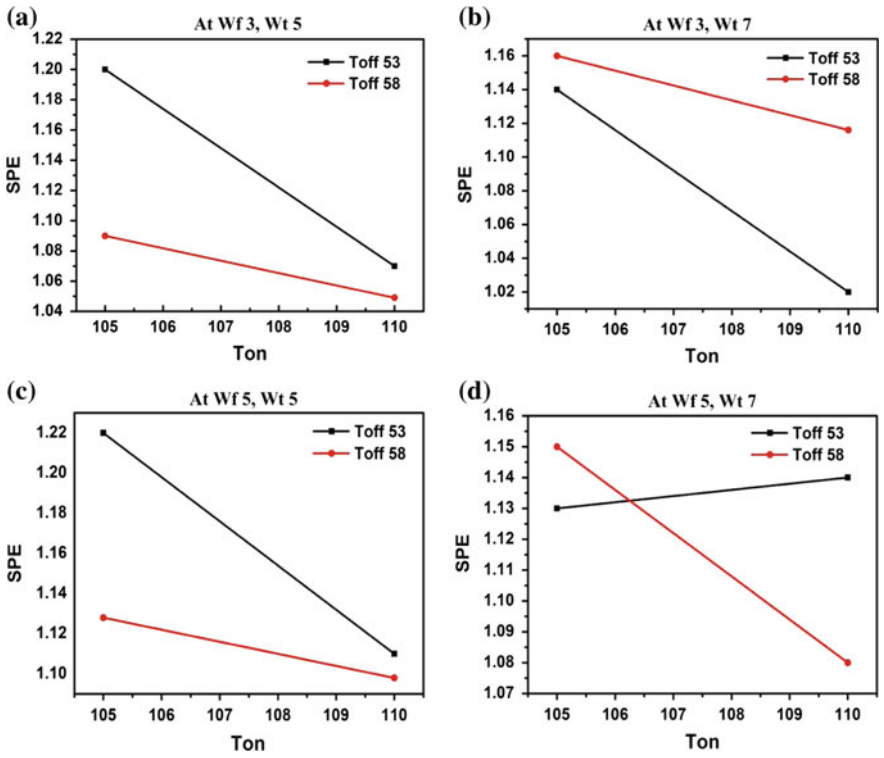

Fig. 19 Effect of single pitch error on process parameters

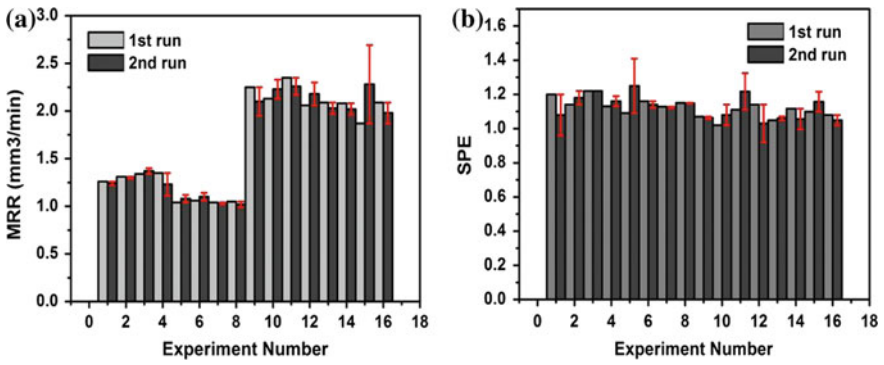

Fig. 20 Error graphs obtained for MRR and single pitch error

Figure 20 depicts the error graphs obtained for both MRR and single pitch error in machining of the gear profile. As the replication is made twice, the error graphs were obtained considering the output responses of the first and second run and it

was observed from both the figures that the error variation for both the responses differs by a very small amount satisfying the stability and accuracy of the model.

7 Conclusions

The study focused on the effect of machining parameters on the output responses of the gear cut copper material in the main cut operation and analysis of surface characteristics by the wire EDM process. Key findings can be summarized as follows.

- The experiment was conducted for the gear cutting process by wire EDM. The response parameters were optimized using MOORA method and a combination was obtained for the best alternative.
- Microscopic study of the material was carried out at the optimized setting of the response and it was found that some grain like structures were formed on the workpiece material after the material has been etched by the etchant, i.e. distilled water and nitric acid.
- Microstructural study also reveals that voids and craters were formed on the surface of the workpiece as viewed under SEM at higher magnification zoom. Micro-voids were formed due to the solidification of the molten material on the material surface. Furthermore holes, debris and cracks were also identified due to high discharge energy settings resulting in high intensity of the spark. Some cracks and melted deposits were also marked over the wire surface at high discharge energy, servo voltage and wire feed rate due to the increase in the induced stresses and peak current exceeding the wires tensile strength.
- EDS characterization was done to know the elemental composition of the machined surfaces and wires. The percentage of copper was found to be 79.32 in the workpiece material. Similarly, the EDS characterization was also performed for the brass wire depicting the weight percentage of copper to be 54.66% and Zznc to be 45.34%.
- ANOVA table and response table were depicted showing that pulse on time and pulse off time were the most significant factors affecting the responses. The regression equations were obtained and the experimental model was validated with the statistical model values illustrating a good sign of stability of the model.
- Various plots like main effect plot for means, surface plots and contour plots were analysed to describe the potential relationship between the variables. The effects of different responses on individual process parameters were plotted and investigated. The graph reveals that the MRR increases and single pitch error decreases with the increase in the pulse on time. The MCR decreases with the increase in the wire feed rate and increases with the increase in the wire tension due to low wire feed rate and high discharge energy drawn from the wire.
- The error graphs were obtained for both MRR and single pitch error and it was observed that the error variation for both the responses differs by a very small

amount satisfying the stability and accuracy of the model. The optimized setting or combination obtained in the present work can be further used in machining and manufacturing of high-quality copper gears.

References

Brauers, W.K.M. 2007. *Optimization methods for a stakeholder society: A revolution in economic thinking by multi objective optimization*. Boston: Kluwer Academic.

Dodun, O., A.M.G. Coelho, L. Statineanu, and G. Nagit. 2009. Using wire electrical discharge machining for improved corner cutting accuracy of thin parts. *Interntional Journal of Advanced Maufacturing Technology* 41: 858–864.

Gupta, K., and N.K. Jain. 2014a. On surface integrity of miniature spur gear manufactured by wire electrical discharge machining. *International Journal of Advanced Manufacturing Technology* 72: 1735–1745.

Gupta, K., and N.K. Jain. 2014b. Analysis and optimization of micro-geometry of miniature spur gears manufactured by wire electric discharge. machining. *Precision Engineering* 38 (4): 728–737.

Gupta, K., N.K. Jain, and R.F. Laubscher. 2015. Spark erosion machining of miniature gears: a critical review. *International Journal of Advanced Manufacturing Technology* 80: 1863–1877.

Habib, S., and A. Okada. 2015. Study on the movement of wire electrode during fine wire electrical discharge machining process. *Journal of Materials Processing Technology* 227: 147–152.

Kanlayasiri, K., and S. Boonmung. 2007. An investigation on effects of wire-EDM machining parameters on surface roughness of newly developed DC53 die steel. *Journal of Materials Processing Technology* 187–188: 26–29.

Kuriakose, S., K. Mohan, and M.S. Shunmugam. 2003. Data mining applied to wire-EDM process. *Journal of Materials Processing Technology* 142: 182–189.

Liao, Y.S., J.T. Huang, and Y.H. Chen. 2004. A study to achieve a fine surface finish in Wire-EDM. *Journal of Materials Processing Technology* 149: 165–171.

Mandal, A., A.R. Dixit, A.K. Das, and N. Mandal. 2015. Modeling and optimization of machining nimonic C-263 super alloy using multi-cut strategy in WEDM. *Materials and Manufacturing Processes* 31 (7): 37–41.

Menz, W. 2003. Micro wire EDM for high aspect ratio 3D microstructuring of ceramics and metals. *Microsystem Technologies* 11: 250–253.

Miller, S.F., A.J. Shih, and J. Qu. 2004. Investigation of the spark cycle on material removal rate in wire electrical discharge machining of advanced materials. *International Journal of Machine Tools and Manufacture* 44: 391–400.

Ming, W., Z. Zhang, G. Zhang, Y. Huang, J. Guo, and Y. Chen. 2014. Multi-objective optimization of 3D-surface topography of machining YG15 in WEDM. *Materials and Manufacturing Processes* 29(5): 37–41.

Plaza, S., N. Ortega, J.A. Sanchez, I. Pombo, and A. Mendikute. 2009. Original models for the prediction of angular error in wire-EDM taper-cutting. *Interntional Journal of Advanced Maufacturing Technology* 44: 529–538.

Qu, J., A.J. Shih, and R.O. Scattergood. 2002. Development of cylindrical wire electrical discharge machining process, part 2: surface integrity and roundness. *Journal of Manufacturing Science and Engineering* 124: 708–714.

Sanchez, J.A., S. Plaza, N. Ortega, M. Marcos, and J. Albizuri. 2008. Experimental and numerical study of angular error in wire-EDM. *International Journal of Machine Tools and Manufacture* 48: 1420–1428.

Taylor, P., K. Gupta, and N.K. Jain. 2013. On micro-geometry of miniature gears manufactured by wire electrical discharge machining. *Materials and Manufacturing Processes* 28: 37–41.

Wentai, S., L. Zhidong, and Q. Mingbong. 2015. Wire tension in high-speed wire electrical discharge machining. *International Journal of Advanced Manufacturing Technology* 82: 379–389.

Yan, M.T., and P.H. Huang. 2004. Accuracy improvement of wire-EDM by real-time wire tension control. *International Journal of Machine Tools and Manufacture* 44: 807–814.

Yan, M.T., and Y.T. Liu. 2009. Design, analysis and experimental study of a high-frequency power supply for finish cut of wire-EDM. *International Journal of Machine Tools and Manufacture* 49 (10): 793–796.

Yeh, C., K. Wu, and J. Lee. 2013. Study on surface characteristics using phosphorous dielectric on wire electrical discharge machining of polycrystalline silicon. *International Journal of Advanced Manufacturing Technology* 69: 71–80.